

Measurement of the Background Activities of a ^{100}Mo -enriched powder sample for AMoRE crystal material using a single high purity germanium detector

Su-yeon Park

Department of Physics, Ewha Womans University, Seoul 03760

Insik Hahn

Department of Science Education, Ewha Womans University, Seoul, 03760

Center for Exotic Nuclear Studies, Institute for Basic Science (IBS), Daejeon, 34126

Woon Gu Kang, Gowoon Kim*, Eun Kyung Lee and Douglas S. Leonard

Center for Underground Physics, Institute for Basic Science (IBS), Daejeon, 34126

Vladimir Kazalov

Baksan Neutrino Observatory, Institute for Nuclear Research of the Russian Academy of Science,

Kabardino-Balkaria, 361609

Yeong Duk Kim and Moo Hyun Lee

Center for Underground Physics, Institute for Basic Science (IBS), Daejeon, 34126

IBS School, University of Science and Technology (UST), Daejeon, 34113

Elena Sala

Center for Axion and Precision Physics Research, Institute for Basic Science (IBS), Daejeon, 34051

The Advanced Molybdenum-based Rare process Experiment (AMoRE) searches for neutrino-less double-beta ($0\nu\beta\beta$) decay of ^{100}Mo in enriched molybdate crystals. The AMoRE crystals must

have low levels of radioactive contamination to achieve a low rate of background signals with energies near the Q-value of ^{100}Mo $0\nu\beta\beta$ decay. To produce low-activity crystals, radioactive contaminants in the raw materials used to form the crystals must be controlled and quantified. $^{100\text{Enr}}\text{MoO}_3$ powder, which is enriched in the ^{100}Mo isotope, is of particular interest as it is the source of ^{100}Mo in the crystals. A high-purity germanium detector having 100% relative efficiency, named CC1, is being operated in the Yangyang underground laboratory. Using CC1, we collected a gamma spectrum from a 1.6 kg $^{100\text{Enr}}\text{MoO}_3$ powder sample, enriched to 96.4% in ^{100}Mo . Activities were analyzed for the isotopes ^{228}Ac , ^{228}Th , ^{226}Ra , and ^{40}K , long-lived naturally occurring isotopes that can produce background signals in the region of interest for AMoRE. Activities of both ^{228}Ac and ^{228}Th were < 1.0 mBq/kg at 90% C.L. The activity of ^{226}Ra was measured to be 5.1 ± 0.4 (stat) ± 2.2 (syst) mBq/kg. The ^{40}K activity was found as < 16.4 mBq/kg at 90% C.L.

PACS number: 23.40.-s, 29.40.-n, 29.30.Kv

Keywords: neutrino-less double beta decay, ^{100}Mo -enriched powder, high purity germanium detector, radioisotope contamination

* E-mail: kkw-owo@hanmail.net (Gwoon Kim)

Fax: +82-42-878-8509

I. INTRODUCTION

Searches for neutrino-less double-beta ($0\nu\beta\beta$) decay in isotopes such as ^{100}Mo can potentially determine if the neutrino is a Majorana particle or not. If the ^{100}Mo $0\nu\beta\beta$ decay occurs, the Q-value energy of 3034.4 keV [1] will be carried away by the two emitted electrons, creating an observable peak in the energy spectrum of a detector. The half-life of the decay is estimated to be longer than 1.1×10^{24} years [2]. To reach sensitivities to $0\nu\beta\beta$ decay at levels at or above this half-life, the rate of background events in the region of interest (ROI) must be less than 10^{-4} count/keV/kg/year [3].

The Advanced Molybdenum-based Rare process Experiment (AMoRE) searches for neutrino-less double-beta ($0\nu\beta\beta$) decay of ^{100}Mo using enriched molybdate crystals. Currently, the full experimental setup, AMoRE-II, is being prepared to observe the decay in detectors constructed with cryogenic crystals containing molybdenum enriched in the ^{100}Mo isotope [4, 5]. Around 200 kg of molybdate crystals will be in operation.

The AMoRE detectors have full width half maximum (FWHM) energy resolutions of about 10 keV, [6] implying an ROI around the Q-value from 3024.4 keV to 3044.4 keV, if defined with a width of twice FWHM. Daughter isotopes of ^{232}Th and ^{238}U decay chains can produce background events in AMoRE in this energy range via multiple mechanisms involving single or coincident emission. In particular, as explained in Ref [7], the ^{212}Bi - ^{212}Po and ^{214}Bi - ^{214}Po decay sequences can produce backgrounds in the ROI. Coincident emissions from ^{208}Tl decay, primarily from 583.2 keV and 2614.5 keV gammas, can also produce signals in the AMoRE ROI.

Two-neutrino double-beta decay of ^{100}Mo can produce electrons with energies up to the Q-value. Sufficiently high-activity decays from radioactive contaminants can potentially create background signals in the ROI through random coincidence between two such decays or between one contaminant decay and a two-neutrino decay. For example, the most energetic decay mode of ^{40}K has a Q-value 1504.4 keV, well below the AMoRE ROI. However, if the activity of ^{40}K in crystals is high enough, it can still result in a signal in the ROI via random coincidence with other activities, including two-neutrino

decay.

Internal background levels of $^{40}\text{Ca}^{100}\text{MoO}_3$ crystals for AMoRE were measured to obtain activities of ^{214}Po from the ^{238}U decay chain and ^{216}Po from the ^{232}Th decay chain [8-10]. AMoRE detector components were also scanned to acquire activities of background contaminants [11, 12]. Based on these data, ^{232}Th and ^{238}U decay chains and ^{40}K decays were simulated to find which parts of the AMoRE detector system contribute significant background signals in the ROI [13]. From previous measurements and simulations in Ref. [8-13], it was found that internal radioactive sources of crystals likely contribute the most to backgrounds in the ROI.

In order to reduce the levels of background contaminants in the crystals, the ^{100}Mo -enriched powder is purified by physical and chemical methods before being used for crystal growth [14]. Monitoring the quality of purification before proceeding to crystal growth is essential. To understand the starting point for this process, we measured activities of contaminants in an unpurified powder sample.

A high-purity germanium (HPGe) detector named CC1 with 100% relative efficiency is located in the Yangyang underground laboratory (Y2L). The underground location, at a depth of 700 m, is used to reduce backgrounds from cosmic radiation [11, 12, 15]. Lead and copper blocks shield CC1. The background level of CC1 is around 0.0078 s^{-1} in the energy range from 50 keV to 4000 keV [15].

The levels of radioactive contamination in a 1.6 kg sample of powder were measured using CC1. We analyzed activities of several radioactive isotopes, including ^{228}Ac , ^{228}Th , ^{226}Ra , and ^{40}K , which can make background signals in the ROI of AMoRE.

II. EXPERIMENTAL SETUP

The germanium crystal of the CC1 detector has a diameter of 81.4 mm and a height of 81.7 mm. The crystal is in an aluminum canister that has an outer diameter of 105 mm and a height of 120 mm. A sample space surrounds the canister. As described in Ref [15], the detector and sample space is

surrounded by a layered shield. The shielding consists of, from inside to out, a 50 mm thick layer of lead, a 100 mm thick layer of copper, and an outer lead shield. The vertical walls of the outermost shield are 150 mm thick, while the upper and lower layers are 100 mm thick. Fig. 1 shows a schematic of the CC1 detection system, including the geometry of the powder sample.

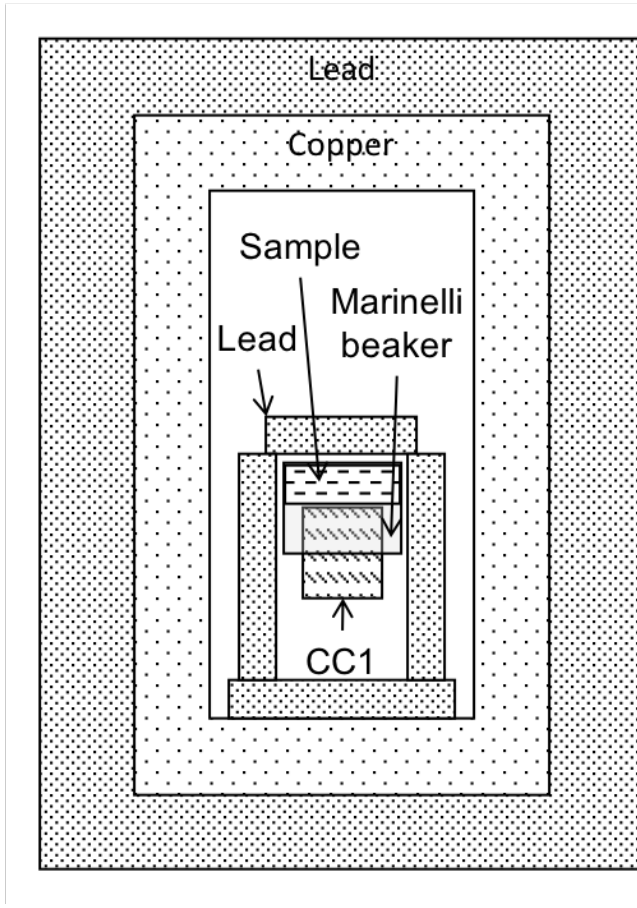


Fig. 1. A schematic of the experimental setup with the CC1 detector system, lead and copper shields, and the powder sample in a Marinelli beaker.

A total of 10 kg of ^{100}Mo -enriched powder was provided by JSC Isotope [16]. The supplier certified that it contains 6.8 kg of molybdenum and that the enrichment level of ^{100}Mo is 96.4%. The ^{100}Mo -enriched powder was divided and packaged into 15 separate plastic bags. Three bags, which weigh 1.6 kg in total, could fit in a Marinelli beaker. The shape and position of the powder sample on CC1 could be

fixed during data taking. The Marinelli beaker containing the powder sample was placed around CC1, as shown in Figs. 1 and 2.

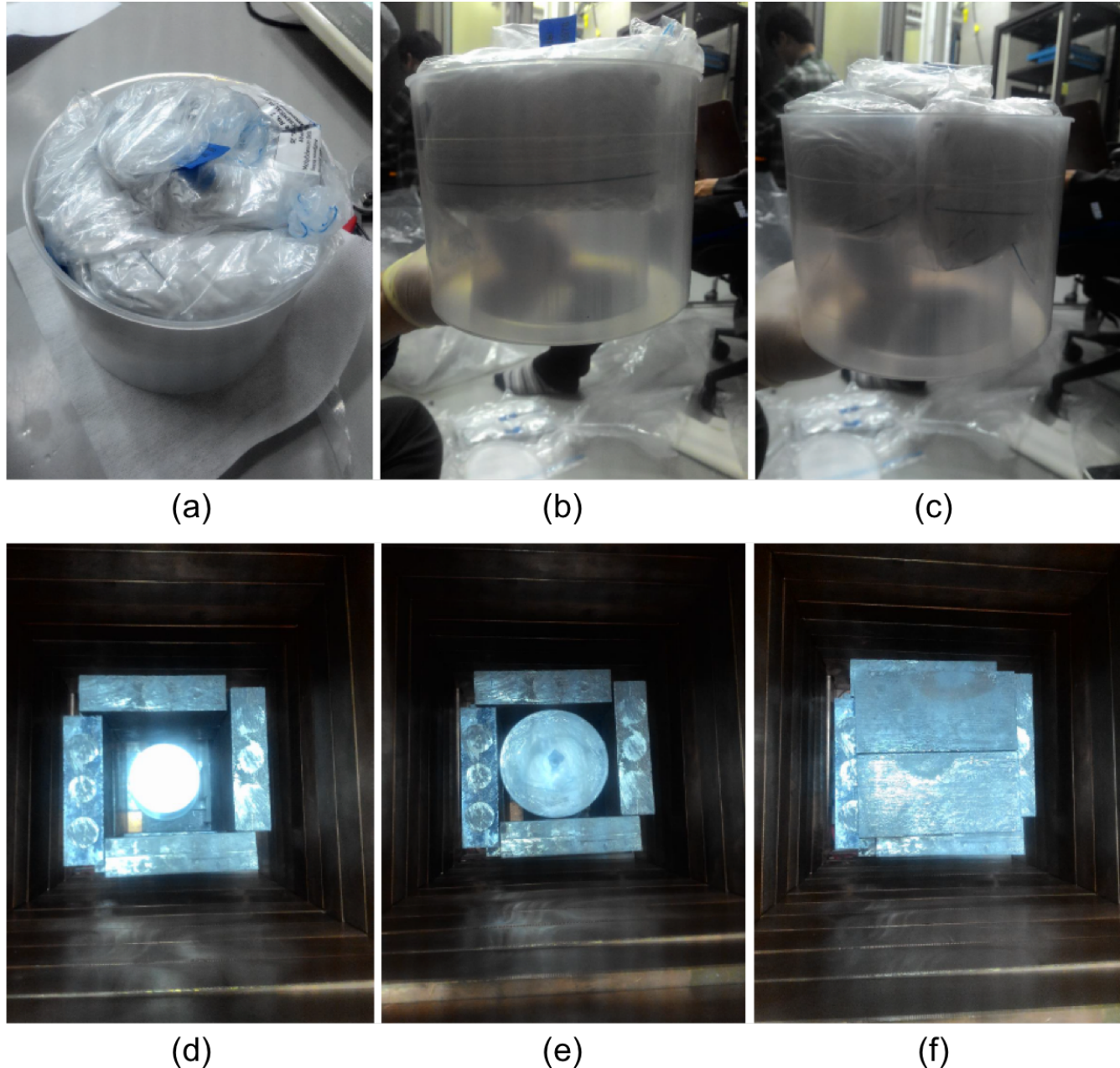


Fig. 2. The powder sample in a Marinelli beaker (a-c) and its installation on CC1 (d-f).

Signals were sent from the pre-amplifier to a shaping amplifier configured with $6 \mu\text{s}$ shaping time.

Signals from the outputs of the shaping amplifier were digitized by a multichannel analyzer and stored to disk for later analysis. The data were collected for 340 hrs.

^{222}Rn gas entering the detection volume from laboratory air can produce background signals for the ^{226}Ra sub-chain. In order to reduce this effect, the detection volume was continuously flushed with boil-off nitrogen gas from a liquid-nitrogen bottle.

In order to subtract signals arising from contaminants in the detector system itself, background data were obtained with the sample space empty, without the presence of the powder sample. The background data and powder data were taken in the same experimental environment and conditions, with, for example, a similar nitrogen gas flushing rate. The total live-time for background data was 807 hrs.

III. ANALYSIS

All of the radioactive decay information used in this analysis were from the National Nuclear Data Center (NNDC) [17]. The detection efficiencies were calculated using GEANT4 Monte Carlo simulations [18].

The energy spectra collected with the powder sample were calibrated using the most probable centroid values from fits to gamma peaks at 186.2 keV from ^{226}Ra decay, 295.2 keV and 352.0 keV from ^{214}Pb , 609.3 keV, 1120.3 keV and 1764.5 keV from ^{214}Bi , and 1460.8 keV from ^{40}K . The peaks were each fitted to a Gaussian distribution function added to a parameterization of the continuum backgrounds caused by Compton scattering. A quadratic function was used to find a relation between ADC channels and energies, as shown in Fig. 3(a).

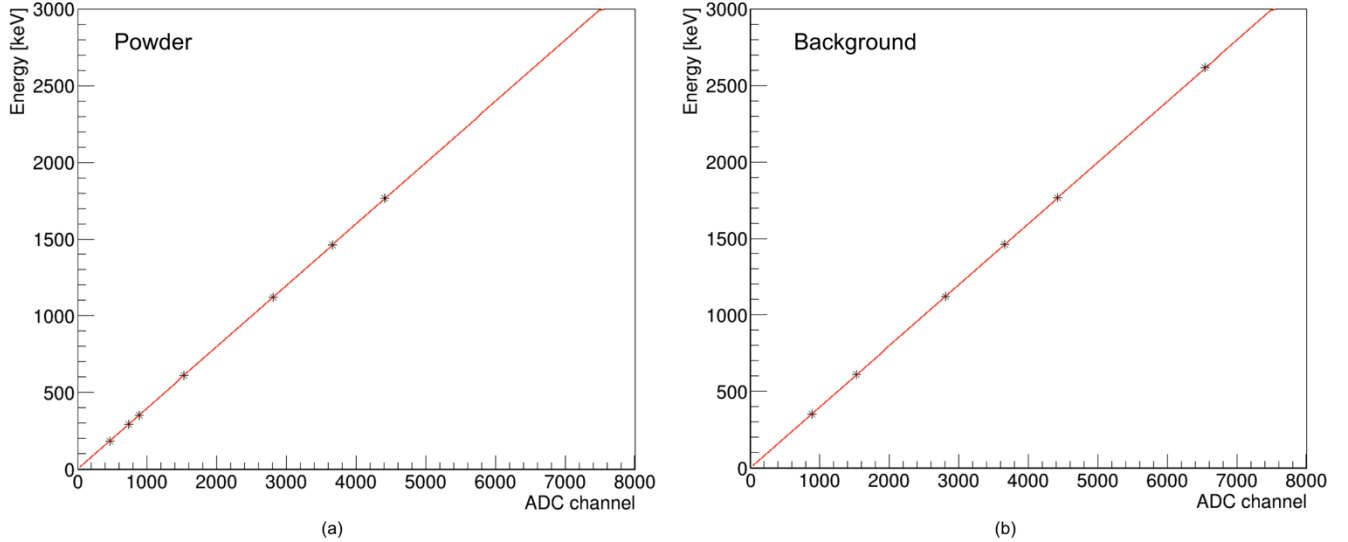


Fig. 3. ADC channel vs. energy with calibration peak points and fitted functions. Quadratic functions were used for calibration fits. (a) is for the powder data and (b) is for the background data.

The calibration function determined for the powder data was

$$Energy [keV] = -0.61 + 0.40 \times ADC + 2.14 \times 10^{-8} \times ADC^2,$$

where ADC means the ADC channel number.

To confirm the uncertainty of the energy calibrations, energies of the observed ^{214}Bi peaks at 609.3 keV and 1120.3 keV were inferred from the calibration and compared to the known values. Peak positions input into the calibration function were obtained from fits in the same way as for the calibration peaks. The inferred energies were lower than the known values by 0.2 keV, a negligible error. The energy resolutions were 1.5 keV at both 609.3 keV and 1120.3 keV (FWHM).

The background data were calibrated with the 352.0 keV, 609.3 keV, 1120.3 keV, 1460.8 keV, 1764.5 keV and 2614.5 keV peaks in the same way. A quadratic function was also used, as shown in Fig. 3(b). The calibration function for the background data was

$$Energy [keV] = -0.92 + 0.40 \times ADC + 3.41 \times 10^{-8} \times ADC^2.$$

Observed positions of 609.3 keV and 1460.8 keV peaks were confirmed in the same way as for the powder data, and differences were 0.2 keV and 0.1 keV lower than the known values, respectively.

Fig. 4 shows the energy spectra of powder data and background data. Energy spectra were divided into six 500 keV regions.

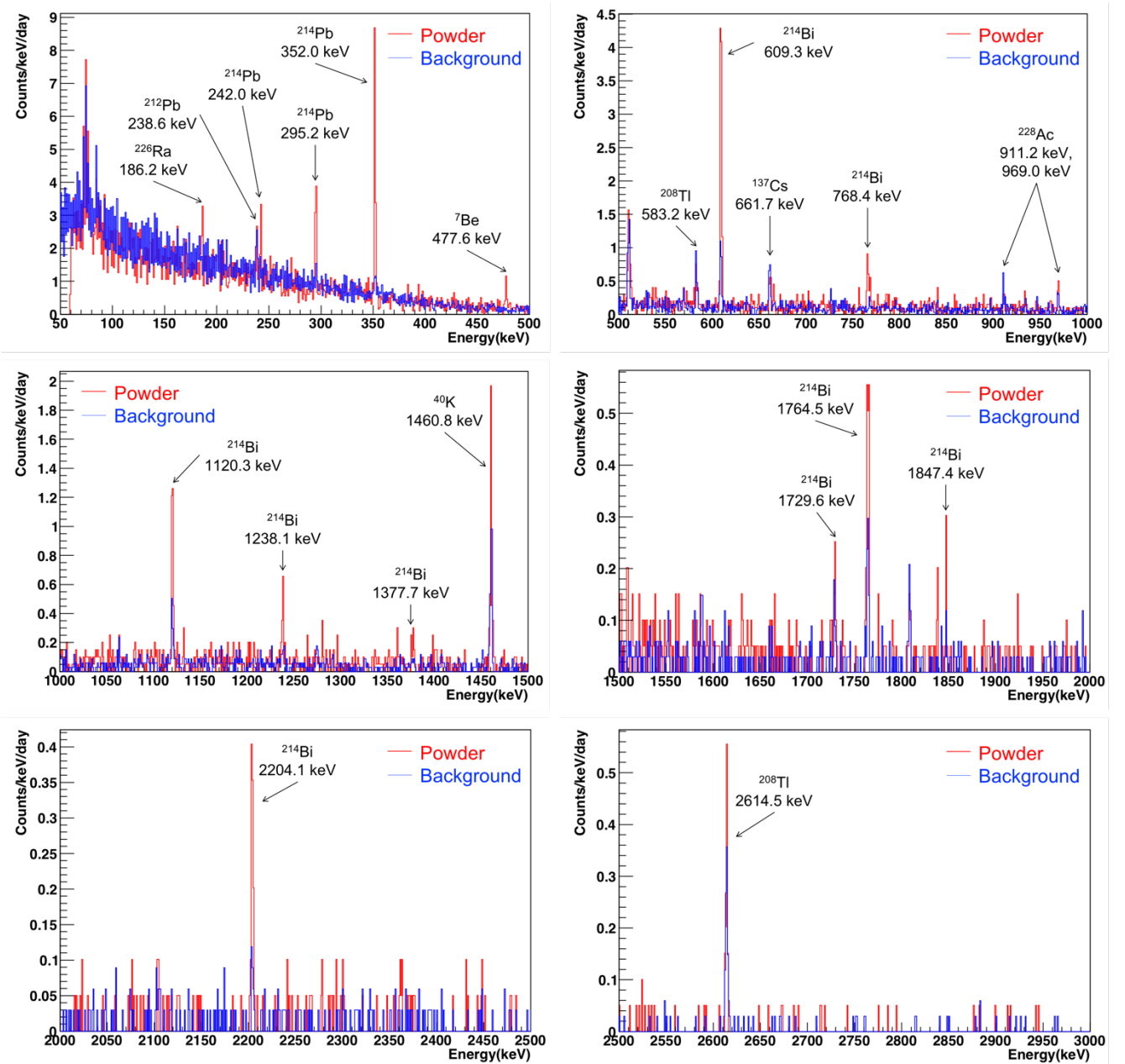


Fig. 4. The energy spectra of the powder data (red) and the background data (blue). Energy spectra were divided into six 500 keV regions. The gamma peaks were indicated with the energies and their mother isotopes.

Most of the marked peaks in Fig. 4 were produced by gamma emissions from decays of ^{228}Ac , ^{228}Th , and ^{226}Ra . The 1460.8 keV peak from ^{40}K was also observed. Activities of these radioisotopes, which can make signals in the AMoRE ROI, were analyzed.

The 477.6 keV peak from the electron capture of ^7Be was also observed. Reactions between secondary cosmic rays and nitrogen or oxygen can produce this isotope [19]. The ^{100}Mo -enriched powder was delivered via a few flights from a production site in Russia to Y2L. We assume that ^7Be in the powder sample was produced as a consequence of the ^{100}Mo -enriched powder's exposure to cosmic rays during the flights. However, the half-life of ^7Be is 53.2 days, which is short compared to the AMoRE-II preparation period, and its Q-value of 861.8 keV is far lower than the AMoRE ROI centered around 3034.4 keV. Therefore, the activity of ^7Be was not analyzed.

3.1 Background activities from labels

Because of logistical constraints, and to avoid contaminating the powder sample or losing any of the valuable material, it was kept in the original bags and fit in a Marinelli beaker. All the bags had labels attached outside, as shown in Fig. 2. When preparing the powder sample, the labels were kept on the bags to avoid damaging or tearing the bags. Three pieces of labels were thus installed together with the powder sample in CC1. The labels were composed of paper and ink, which can both contain relatively high levels of radioactive contaminants. Contributions from these activities should be subtracted from the observed count rates. When the powder sample was later processed for purification at a separate facility, the labels were retrieved. Several samples of labels were then assayed using CC1. Fig. 5 shows some of the label samples. The activities obtained from these assays, in mBq/pc, are summarized in

Table 1.



Fig. 5. For subtracting the contributed counts of gammas from the labels in the powder data, the activities in a label sample was measured on CC1. (a) Labels in plastic bags are vacuum sealed and (b) the samples are placed on CC1 for the activity measurement.

Isotope	^{228}Ac	^{228}Th	^{226}Ra	^{40}K
Activity [mBq/pc]	0.06 ± 0.03 (< 3.8 at 90% C.L.)	0.07 ± 0.02	2.3 ± 0.1	0.9 ± 0.2

Table 1. Measured activities of various isotopes in the representative label samples in units of mBq/piece.

Three labels (pieces) in total were installed together with the powder sample.

The measured label activity values were used to estimate the contributions by the label contaminations to the peak rates observed in the powder activity measurement. Uncertainties from these contributions were also considered. For a particular peak from a particular activity, the number of counts C_L contributed

by the labels during the measurement time T_P of the powder sample was determined as:

$$\frac{c_L}{T_P} = A_L \times \varepsilon_L \times N_L \times B.R. \times G.I.,$$

where A_L is the observed specific activity of the labels in Table 1, ε_L is the full-energy detection efficiency for a gamma of interest produced from random locations within the labels during the powder activity measurement, N_L is the number of labels included in the powder activity measurement, $B.R.$, is the branching ratio for the isotope in question, and $G.I.$ is the gamma intensity.

3.2 Detection efficiency and simulation

To determine detection efficiencies, decay chains of ^{232}Th and ^{238}U , as well as decays of ^{40}K , were simulated in the powder and labels using the GEANT4 simulation toolkit. Full decays were simulated including coincident gamma emission. Geometries of the CC1 detector system, the powder sample, the labels, and the Marinelli beaker were included in the simulation. Details are shown in Fig 6.

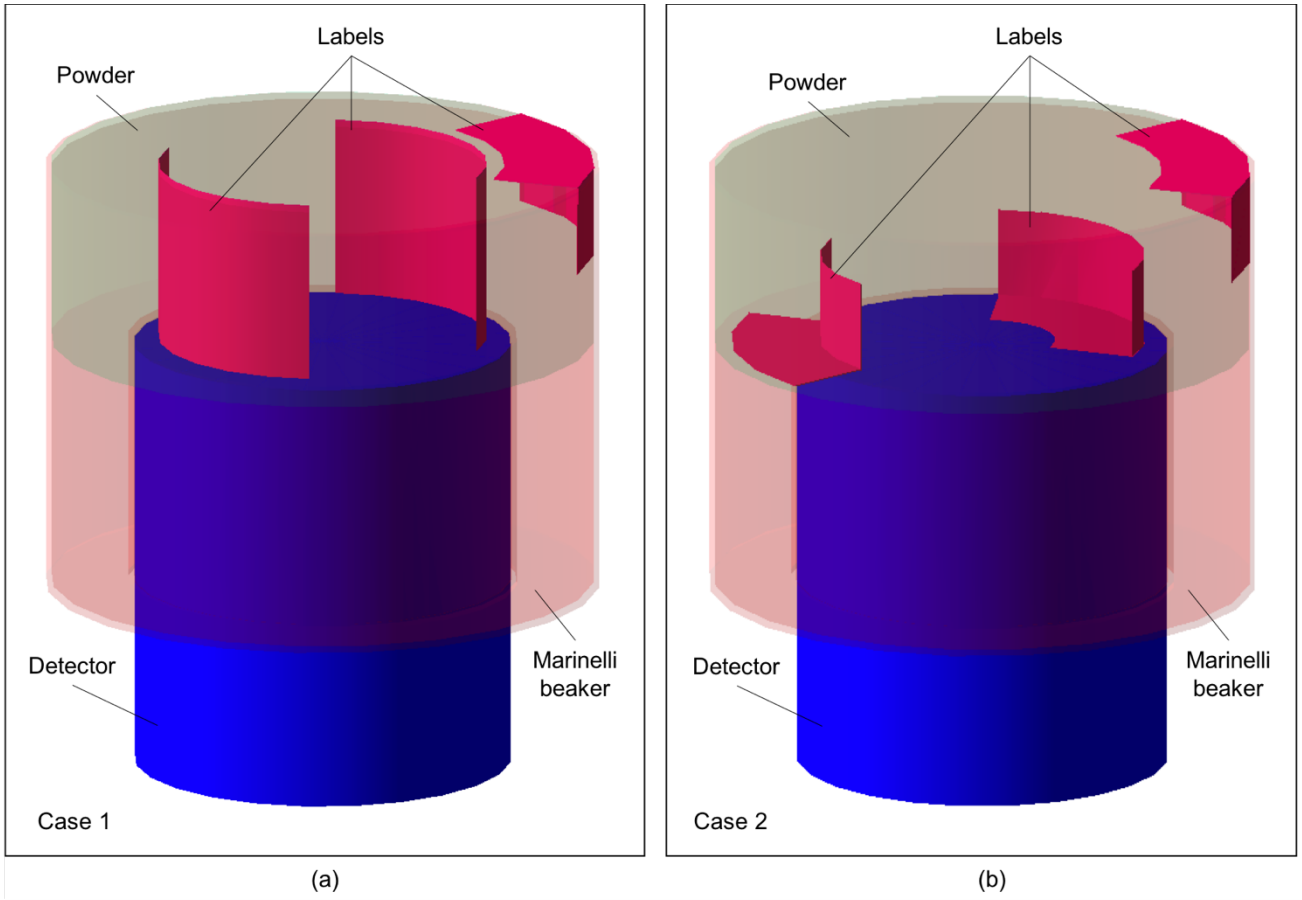


Fig. 6. Two different simulated geometries for the powder sample and the labels in a Marinelli beaker on CC1. (a) shows the geometry of case 1, which gave the minimum detection efficiency values for the label contaminants, and (b) shows that of case 2, which produced the maximum values. Blue one is the CC1 detector cryostat. The Marinelli beaker is shown in pink. Transparent dark green represents the powder sample. The three red items are the labels.

Detection efficiency, ε , of a gamma with emitted energy E is calculated as

$$\varepsilon = \frac{N_d}{N_g},$$

where N_d is the area of the Gaussian distribution, in units of counts, determined from the fit to the full-

energy peak at E , and N_g is the number of gammas generated with energy E . Gammas were generated in random locations within the geometry of the powder sample. For the purpose of subtracting contributions from the labels, the simulation of decays in the labels was generated separately.

Because the positions and shapes of the labels were not fully recorded, a few sample-installation cases that represent the extreme possibilities for label detection efficiency were simulated. From photos in Fig. 2, one label faced outward and was folded in half. The exact orientations of the other labels are not known. Through a combination of straight and folded labels, four representative geometrical cases were considered. All of them were simulated, and the two cases that gave the minimum and the maximum detection efficiencies are shown in Fig. 6. The simulation using case 1 resulted in the minimum detection efficiencies for radioactive contaminants in the labels, and that of case 2 produced the maximum values.

Table 2 lists detection efficiencies of the powder sample ε_p and the labels ε_L .

Isotope		Energy [keV]	Detection efficiency (%)			
			Case 1		Case 2	
			ε_p	ε_L	ε_p	ε_L
^{228}Ac	911.2	911.2	1.7	1.2	1.6	2.4
	969.0	969.0	1.6	1.2	1.6	2.3
^{228}Th	^{212}Pb	238.6	5.1	2.8	2.8	2.8
	^{208}Tl	583.2	2.6	1.9	1.9	1.9
		2614.5	1.0	0.8	0.8	0.8
^{226}Ra	^{214}Pb	295.2	5.3	3.1	3.1	3.1
		352.0	4.4	2.8	2.8	2.8
	^{214}Bi	609.3	2.7	1.9	1.9	1.9
		1120.3	2.0	1.5	1.5	1.5
		1764.5	1.8	1.3	1.3	1.3
	^{40}K	1460.8	1.4	1.1	1.3	2.0

Table 2. Simulated detection efficiencies ε_p and ε_L for the powder sample and labels, respectively, for two simulation cases representing the extremes in the possible label positions.

Dead layers, inactive volumes in a germanium crystal, act like shielding layers and reduce the detection

volume of the germanium [20]. For this reason, the efficiency was calibrated with a multi-nuclide source with known activities. The simulation geometry of the CC1 detector system was fine-tuned to produce efficiencies matching the multi-nuclide source data. After tuning the simulation, the discrepancy between the calibration data and the simulation was found to be less than 10% [12]. For simulation studies of similar measurements, we have found that sample geometry errors contribute at most a few percent. We include a 10% systematic error to account for calibration discrepancies and sample geometry errors.

3.3 Count and activity

A parent activity A_P from the powder sample derived from any single gamma peak in one of the decay-chain isotopes is given by

$$A_P = \frac{\frac{C_O}{T_P} - \frac{C_L}{T_P} - \frac{C_B}{T_B}}{\varepsilon_P \times M_P \times B.R. \times G.I.},$$

where C_O is peak counts observed in the powder data, C_L is the estimated contribution to C_O from contaminations in the labels, C_B is peak counts observed in the background data, T_B is the measurement time of the background data, and M_P is the mass of the powder sample.

The background activities in the powder sample were analyzed with the two maximally different detection efficiency scenarios described above, and the results for each were obtained. Two isotopes of ^{228}Th and ^{226}Ra were assumed to be in equilibrium with their respective decay chains, a good assumption given the short half-lives of the decay-chain daughters. With this assumption, all activities in the ^{228}Th or ^{226}Ra sub-chains were, with appropriate branching ratios applied, assumed to be valid measures of the respective parent activities. Results from the same chain were thus averaged together. Differences between the minimum and the maximum activity results were used for an estimate of geometrical uncertainty in the contribution from the label contaminants.

Table 3 lists the counts in gamma peaks from ^{228}Ac , ^{228}Th , ^{226}Ra , and ^{40}K for the powder data and the background data. Table 4 lists the analysis results using the two most extreme simulation cases.

Isotope	Energy [keV]	Rate [$\times 10^{-2}$ counts/hour]			
		C_O/T_P	Case 1	Case 2	C_B/T_B
			C_L/T_P	C_L/T_P	
^{228}Ac	911.2	2.9 ± 1.3	0.21 ± 0.09	0.40 ± 0.17	3.5 ± 0.8
	969.0	4.4 ± 1.5	0.13 ± 0.05	0.23 ± 0.10	2.3 ± 0.7
^{228}Th	^{212}Pb	238.6	11.4 ± 3.1	0.64 ± 0.14	1.62 ± 0.36
	^{208}Tl	583.2	5.2 ± 1.9	0.32 ± 0.07	0.59 ± 0.13
		2614.5	6.2 ± 1.3	0.18 ± 0.04	0.27 ± 0.06
^{226}Ra	^{214}Pb	295.2	37.2 ± 2.5	10.2 ± 0.5	24.4 ± 1.3
		352.0	70.4 ± 3.0	17.6 ± 0.9	39.5 ± 2.1
	^{214}Bi	609.3	53.9 ± 2.6	16.8 ± 0.9	30.3 ± 1.6
		1120.3	16.7 ± 2.5	4.4 ± 0.2	7.4 ± 0.4
		1764.5	10.3 ± 1.8	3.8 ± 0.2	6.7 ± 0.4
		40K	19.6 ± 2.6	1.1 ± 0.2	1.9 ± 0.4
		1460.8			10.5 ± 1.2

Table 3. Peak rates for activity analysis. For each gamma peak, C_O is the total observed number of counts in the full-energy peak from the powder data, C_L is the estimated contribution to C_O from contaminations in the labels, and C_B is counts from the background peak intrinsic to the detector construction. For comparison, counts are normalized to acquisition times T_P (340 hrs) and T_B (807 hrs) for powder and background data, respectively.

Isotope	Activity \pm statistical uncertainty [mBq/kg]	
	Case 1	Case 2
^{228}Ac	0.06 ± 0.52	0.001 ± 0.535
^{228}Th	0.3 ± 0.4	0.2 ± 0.4
^{226}Ra	6.9 ± 0.3	3.4 ± 0.4
^{40}K	9.5 ± 3.3	8.6 ± 3.4

Table 4. Activities of various isotopes in the powder sample derived using two different simulations for label contamination efficiencies based on the most extreme possible arrangements of the labels.

IV. RESULTS AND CONCLUSIONS

Table 5 summarizes the background activity results of the powder sample. The observed activities for ^{228}Ac , ^{228}Th , and ^{40}K , are found to be within 3σ of zero and are reported as upper limits. The limits were calculated conservatively using the label geometry assumption that resulted in the highest activities. This assumption is represented by the case 1 activities shown in Table 4. An additional systematic uncertainty of 10% is attributed to other efficiency simulation errors. The activities of both ^{228}Ac and ^{228}Th were $< 1.0 \text{ mBq/kg}$ at 90% C.L. The activity of ^{40}K was $< 16.4 \text{ mBq/kg}$ at 90% C.L.

Isotope	Activity [mBq/kg]
^{228}Ac	< 1.0
^{228}Th	< 1.0
^{226}Ra	$5.1 \pm 0.4 \text{ (stat)} \pm 2.2 \text{ (syst)}$
^{40}K	< 16.4

Table 5. Results of activity analysis for the isotopes that can make background signals in the AMoRE-II ROI. Limits at 90% C.L. are shown for results consistent with zero at the 3σ level.

Considering possible configurations of labels and their contaminants, the minimum and the maximum ^{226}Ra activities were, as shown in Table 4, $3.4 \pm 0.4 \text{ (stat)} \text{ mBq/kg}$ from case 2 and $6.9 \pm 0.3 \text{ (stat)} \text{ mBq/kg}$ from case 1. The average result for the ^{226}Ra activity was $5.1 \pm 0.4 \text{ (stat)} \pm 2.2 \text{ (syst)} \text{ mBq/kg}$. The statistical uncertainty is conservatively selected from the larger of the two cases considered. The systematic uncertainty is dominated by half of the difference in the results from the two cases considered and presented in Table 4. Additionally, a 10% detection efficiency uncertainty was included in both label and powder activity measurements.

We report a positive observation for the ^{226}Ra activity in spite of the superficial appearance that the result does not pass our stated 3σ criteria. The label geometry errors dominate the systematic uncertainty. This uncertainty accounts for the full range of possible detection efficiencies from different possible configurations of the labels, and as such is not a Gaussian uncertainty.

For application to AMoRE-II, the most crucial goal of this measurement was to constrain the activity of ^{208}Tl from the ^{228}Th chain. Only upper limits were found for all activities, except for ^{226}Ra . These limits were dominated by statistical uncertainties determined by detector sensitivity, counting time, and limits on sample mass. An array of fourteen HPGe detectors named CAGe, having better-combined sensitivity than CC1, was installed in Y2L [11, 15, 21, 22]. Currently, in order to improve measurements of ^{208}Tl and other activities, other powder samples are being assayed with the CAGe. Other cosmogenic isotopes, such as ^{88}Y [23, 24], may be investigated as well.

Acknowledgment

This work was supported by the Institute for Basic Science (IBS), funded by the Ministry of Science and Technology, Korea (Grant id: IBS-R016-D1).

REFERENCES

- [1] S. Rahaman *et al.*, Phys. Lett. B **662**, 111 (2008).
- [2] A. S. Barabash and V. B. Brudanin, Phys. Atom. Nucl., **74**, 312 (2011).
- [3] V. Alenkov, arXiv:1512.05957v1 [physics.ins-det] (2015).
- [4] H. K. Park, Nucl. Part. Phys. Proc. **273**, 2630 (2016).
- [5] V. Alenkov *et al.*, Eur. Phys. J. C **79**, 791 (2019).
- [6] G. B. Kim *et al.*, Adv. High Energy Phys. **2015**, Article ID 817530 (2015).
- [7] G. B. Kim, PhD. Dissertation, Seoul National University, 2016.
- [8] J. H. So *et al.*, IEEE Trans. Nucl. Sci **59**, 2214 (2012).
- [9] J. Y. Lee *et al.*, IEEE Trans. Nucl. Sci **63**, 543 (2016).
- [10] J. Y. Lee *et al.*, IEEE Trans. Nucl. Sci **65**, 2041 (2018).
- [11] M. H. Lee *et al.*, PoS ICHEP2018 363 (2018).

- [12] E. Lee *et al.*, PoS ICHEP2018 809 (2018).
- [13] A. Luqman *et al.*, Nucl. Instrum. Meth A **855**, 140 (2017).
- [14] O. Gileva *et al.*, J Radioanal Nucl Chem **314**, 1695 (2017).
- [15] G. Kim, Ph.D. Dissertation, Ewha Womans University, 2019.
- [16] JSC isotope, <http://www.isotop.ru/en/>
- [17] National Nuclear Data Center, <https://www.nndc.bnl.gov/nudat2/>
- [18] S. Agostinelli *et al.*, Nucl. Instrum. Meth A **506**, 250 (2003).
- [19] M. Yoshimori *et al.*, Adv. Space Res. **32** 2691 (2003).
- [20] Glenn F. Knoll, *Radiation Detection and Measurement* (John Wiley and Sons, 2000), Ed. 3, Chap. 12, p. 413.
- [21] E. Sala *et al.*, AIP Conference Proceedings **1672**, 120001 (2015).
- [22] E. Sala *et al.*, Journal of Physics: Conference Series **718**, 062050 (2016).
- [23] A. N. Annenkov *et al.*, Nucl. Instrum. Meth A **584**, 334 (2008).
- [24] S. Y. Park *et al.*, PoS ICHEP2018 783 (2018).